5th International Conference on Biaxial/Multiaxial Fatigue and Fracture
Cracow'97, Poland

Hyun-Woo Lee, Se-Jong Oh and Woo-Hyun Choi

Damage Estimates Under Biaxial Random Load Spectrums by Considering Crystal Structure Dependence

Keywords: Damageable plane, Planar slip material, Biaxial non - proportional loading, Additional damage, Crystal structure dependence

ABSTRACT: Additional damage developed from non-proportional biaxial loading was studied and the effects of crystal structures on the damages were investigated. Fractogrphies of Al7075-T651 alloys(F.C.C) and AISI 1045 steels(B.C.C) showed that the directions of slip lines are different from one another, depending on the loading conditions and crystal structures. Under biaxial in-phase loading condition, slips occur almost uni-directionally. But under biaxial out-of-phase or non-proportional loading conditions, slip lines are reciprocally crossed to the wide range of directions. To investigate the crystal structure effects on the damage for biaxial fatigue, three different load path which give the same amount of maximum strain to the directions of slip lines were selected from the information of fractographies. And the test results showed almost the same fatigue life from the statistical point of view under the three different load paths. From these results, the addtional damage due to the non-proportional loading were mainly related with the slip mechanism and so crystal structures. In this study, for the biaxial fatigue, the damage model related with crystal structure is proposed. The comparison of fatigue life between test results and the calculated results from the proposed damage model shows the close correlation with accuracy of 50-200% for various loading conditions

Introduction

Fatigue failure is one of the most common failure modes of metallic structural/mechanical components. Cracks initiate at highly stressed region due to cyclic loading, and their subsequent propagation could lead to failure of the component or structure as a whole. Often the leading may result in a multiaxial stress state, and the stress/strain components may vary in a non-proportional (or out-of-phase) manner. This non -proportionality of loading condition can induce more material damage in comparison to a proportional load path in a plastically deformed material.To account for the extra damage, various kinds of models were proposed[1-6]. Doong & Socie[7] reported that the material dependence of non-proportional hardening behavior results from the difference in dislocation slip modes. Wavy-slip material exhibits the same degree of hardening under both proportional and non-proportional loading. Planar or wavy/planar slip materials increase their hardening during non-proportional loading as the result of the change in dislocation structures. G. Cailletaud et al[8] reported that the extra hardening observed in 316L stainless steel is related with an increase in both slip activity and the formation of abundant mechanical micro-twins. From these results, it is concluded that the extra hardening and damage are due to slip mechanism and this slip mechanism depends on crystal structure. In this study, experimental results are

given for Al7075-T651 alloys(F.C.C) and AISI 1045 steels (B.C.C). The extra-damage due to non-proportional loading path effects was accounted by the proposed damage mechanism. Life predictions under biaxial random loads were performed and compared with experimental results.

Damage mechanism

In the case of a single crystal which receive external load, the slips occur in the most highly densed direction. And the direction depends on crystal structure. The chemical compositions of Al7075-T651 and AISI 1045 steels are given in Table 1.

Table 1. Principal chemical component of Al7075-T651 alloy & AISI1045 steel.

Materials	Al7075-T651	AISI1045 steel
Principal components (%)	Al : 90.1 Zn : 5.6	Fe : 98.8 C : 0.44

The principal component of Al7075-T651 is aluminium and the crystal structure of aluminium is F.C.C(Face Centered Cubic). F.C.C crystal structure has 12 slip systems[9] and the maximum possible number of slip lines on the surface of tubular specimen is 4(0°, 45°, 90°, 135°)[Fig.1(a)].The principal component of steel is Fe and the crystal structure is B.C.C(Body Centered Cubic). B.C.C crystal structure has 48 slip systems and the maximum possible number of slip lines on the surface of specimen is 12(0°,1°,30°,49°, 60°,71°,90°,109°,120°,131°,150°,159°)[Fig.1(b)]. The proposed damage mechanism of a single crystal is given in Fig.2. This mechanism assumes that the damage is accumulated only in damageable planes and the crack surfaces are formed by the connection of these damageable planes. The damageable plane is the same concept aswith glide plane in a single crystal. The direction of macroscopic crack is the same as that of maximum shear strain. It means that though it could be assumed as macroscopically isotropic, but actually it is microscopically anisotropic.Metal material is a group of crystal grains. A material is a polycrystal and each crystal has its own damageable plane[Fig.3]. If uni-axial or biaxial in-phase load was applied to these crystals, some crystals receive maximum damage. The reason for this limited damage is that the only damageable plane whose direction was parallel with maximum shear strain receives maximum damage. But biaxial out-of-phase or non-proportional load is applied

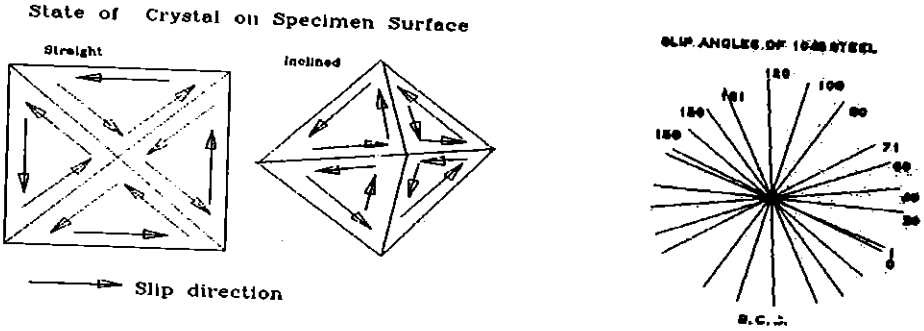

(a) F.C.C(Al7075-T651)

(b) B.C.C(1045 steel)

Fig.1 Slip lines of the given crystal structure

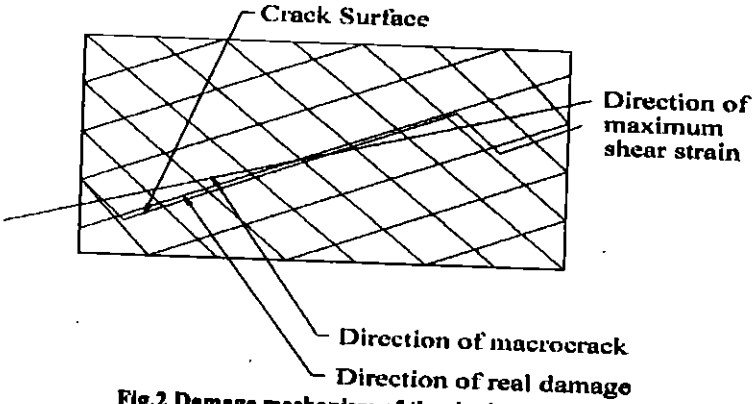

Fig.2 Damage mechanism of the single crystal

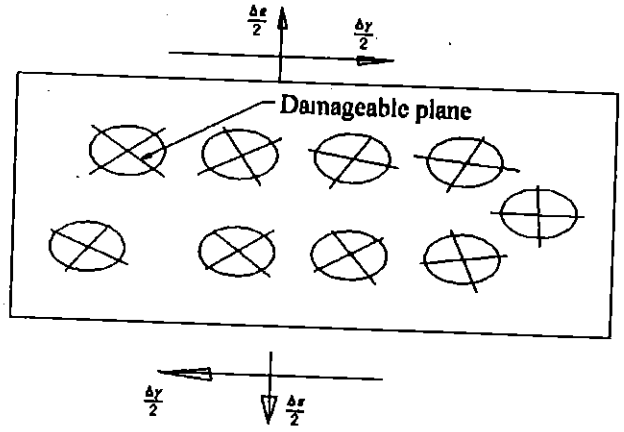

Fig.3 State of the damageable plane

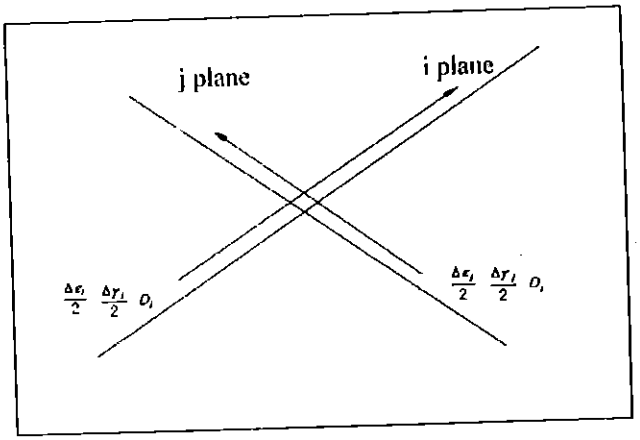

Fig.4 Shear strain and normal strain component at the damageable plane

to these crystals,and all crystals receive maximum damages, because the direction of maximum shear strain was rotated with the applied load. So, every damageable plane receives a maximum shear strain. It is the reason for which the extra damage causes on the materials. To account for this additional damage, a new damage mechanism was proposed[Fig. 1-3].

Damage estimation

To account for the damage D due to crystal structure dependence, the following damage equation(Equation 1) can be considered[Fig. 4].

$$D = \sum_{i=1}^{n} D_i \tag{1}$$

Where D_i is a damage from the given parameter($\Delta\gamma_i$ or given parameter based on multiaxial damage theory) on i-th damageable plane, and it is computed from torsional LCF(low cycle fatigue) test data. The predicted fatigue life N_{predic} is computed by the equation (2):

$$N_{predic} = \frac{1}{D} \tag{2}$$

Parameters

Parameters used for damage estimation are given in equation (3), (4) and (5) for several models. Equation(3) is based on maximum shear strain theory, Equation(4) was proposed

by Brown, Miller & Kandil, and Equation(5) was Brown and Miller's.

$$C_{TRESCA} = \frac{\Delta\gamma}{2} \tag{3}$$

$$C_{BMK} = \frac{\Delta\gamma}{2} + K\varepsilon_n \tag{4}$$

$$C_{elp} = \sqrt{(\frac{\Delta\gamma}{2})^2 + (\rho\varepsilon_n)^2} \tag{5}$$

Where K=1.0 for AISI1045 steel and 1.34 for Al7075-T651
p=1.0 for AISI1045 steel and 1.46 for Al7075-T651

Experimental program

The materials used were tempered Al7075-T651 alloy and hot-rolled 1045 steel. The grain direction of the specimens is longitudinal. Tests were conducted on a servo-controlled closed loop tension torsion machine[Fig.5]. A processor/interface was used for computer control, data acquisition and data reduction. The operating frequency for biaxial tests ranged from 0.05 to 1.0 Hz. The thin-walled tubular specimens with 12.5mm(9mm inside diameter and 1.75mm wall thickness) were used[Fig. 5]. The both sides of each specimen were polished. Standard machine collects were used to grip the ends of each specimen.Tests were performed at room temperature. These materials are commonly used for aircraft and mechanical structures. The mechanical properties of the material tested are given in Table 2. Failure was defined as 10%(Al7075-T651, cyclic hardening) or 50%(1045 steel, cyclic softening) axial load drop in the axial and combined axial-torsional tests, while 10% or 50% torque drop was defined as final failure in the torsional tests. Fatigue tests were conducted under axial, torsional, biaxial in-phase, biaxial out-of-phase, designed biaxial equivalently damageable and biaxial random load path. The test data under axial, torsional and biaxial in-phase and 90 degree out-of-phase loading condition of Al7075-T651[10] were obtained from pre-study and these of 1045 steel were obtained from reference[11].

Table 2. Mechanical properties of Al7075-T651 alloys and AISI1045 steels.

Materials	Yield stress (MPa)	Modulus of elasticity (MPa)	Yield strain	Ultimate strength (MPa)
AISI1045	380	204,000	0.0019	621
Al7075-T651	409	74,742	0.0074	580

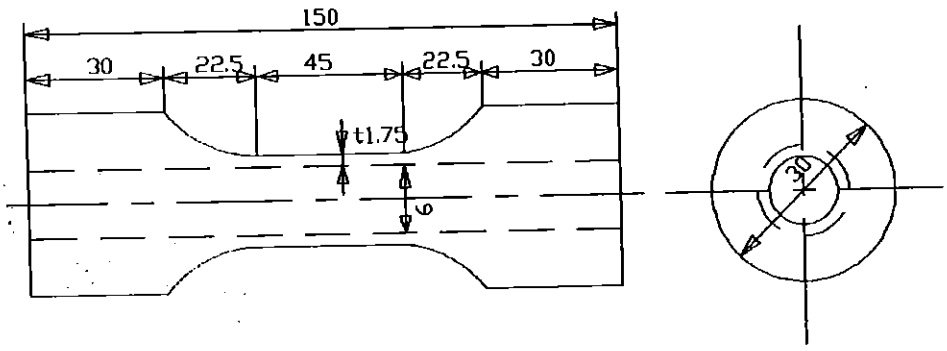

(a)

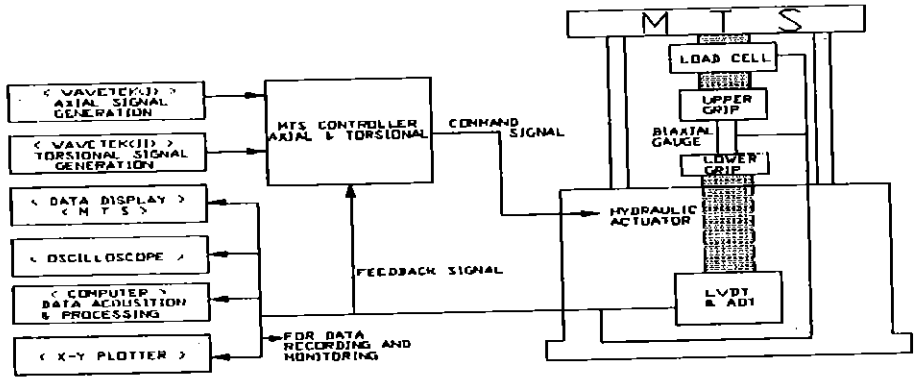

(b)

Fig.5 (a) Geometry of tubular specimen. (b) MTS fatigue test system.

To account for crystal structure dependence of a material damage, the pictures of damaged specimen surface were obtained by SEM(Scanning Electron Microscope)(Al7075-T651 : Fig.6-9, 1045 steel : Fig.10-11). The pictures were sampled at the specimen's outside surface of uncracked position. To clarify the crystal structure dependence on biaxial low cycle fatigue, three different circular load paths and three different rectangular load paths(Fig. 12) were applied to the tubular specimen of Al7075-T651. These load path were designed to get the same amount of fatigue damage. These designed load path were obtained from the proposed damage mechanism and the relative angles between appeared slip lines(damage lines). Biaxial variable sinusoidal and random load paths were applied to the tubular specimen of 1045 steel. The variable sinusoidal load paths were obtained from the Eq.(6) and Eq.(7). The variable random load paths were obtained from the Eq.(8) and Eq.(9).

$$\varepsilon(t) = a_1 \sin(\omega t) + a_2 \sin(3\omega t + \pi/4) + a_3 \sin(9\omega t + \pi/6) \quad (6)$$

$$\gamma(t) = b_1 \cos(\omega t) + b_2 \cos(5\varpi t) + b_3 \cos(7\varpi t) \quad (7)$$

$$\varepsilon(t) = R(t) \tag{8}$$

$$\gamma(t) = R(t) \tag{9}$$

where, $a_1 : a_2 : a_3 = 3 : 2 : 1$, $b_1 : b_2 : b_3 = 3 : 2 : 1$

$R(t)$: random number of range from -1 to 1

$\varepsilon(t)$: Axial strain

$\gamma(t)$: Torsional strain

Discussion

Specimen Observation and Damaged Direction

Axial-loaded Al7075-T651 specimen[Fig.6] shows single direction of slip lines. Slip lines which had relative angle of 80 degree with principal slip lines hardly appear. The relationship between the direction of damageable planes and that of maximum shear strain is given in Fig. 6b. The direction of a damageable plane is parallel with that of maximum shear strain. In-phase loaded(λ = 1) Al7075-T651 specimen[Fig.7] shows two directions of principal slip lines. The angle between two classes of lines is 6 degree. In this case, the direction of maximum shear strain was placed between A and B damageable planes(Fig. 7b). And the amplitude of strain range on each damageable plane is similar. Slip lines which had relative angle of 62 degree with principal slip lines hardly appear. 90 degree out-of-phase loaded Al7075-T651 specimen(λ = 1,2, Fig. 8,9) shows different types of slip lines. In the case of λ =2, the surface of the damaged specimen shows 4 different slip lines. The relative angles are 3-8°, 30-40°, 80-100° and 130-140°.Furthermore, Al7075-T651 has a FCC crystal structure. The state of maximum shear strain at damageable plane is given in Fig.8b. In the case of λ =1, the surface of damaged specimen also shows 4 different slip lines. But the slip lines will not be observed clearly. It means that the amplitude of maximum shear strain was changed with applied loading path. The state of applied strain at damageable plane is given at Fig. 9b. The principal direction of slip lines is scattered near 0°,45°,90°, 135° in the case of Al7075-T651(F.C.C crystal structure) which has 12 slip systems. A single crystal is inclined to the surface of specimen and only 2 dimensional observations were possible. So, the appearing classes of slip lines are 4.In-phase loaded(λ = 1) 1045 steel specimen[Fig.10] shows two or three directions of principal slip lines. The angles between slip lines are less than 30 degree. Slip lines which had relative angle of 71° with principal slip lines hardly appear. 90 degree out-of-phase loaded 1045 steel specimen(λ = 1, Fig. 11) shows different types of slip lines. In the case of λ=1, the surface of the damaged specimen shows only 4 different slip lines. The relative angles are 0°, 30-40°, 90° and 150°. But BCC crystal has 48 slip systems and observable slip lines are 12. The reason for this small appearance in occurrence is from small plastic deformation. From these fractographic observations, the existence of these slip lines

supports the possibility of crystal structure dependence on material damage.

Fig.6A Slip lines under axial load.

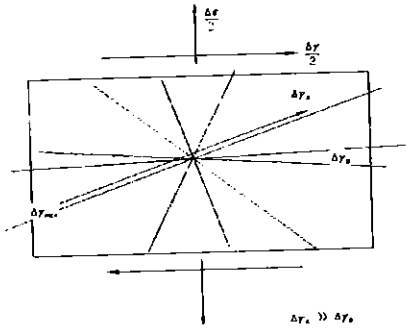

Fig.6B State of strain at damageable plane under axial load.

Fig.7A Slip lines under in-phase load(λ =1).

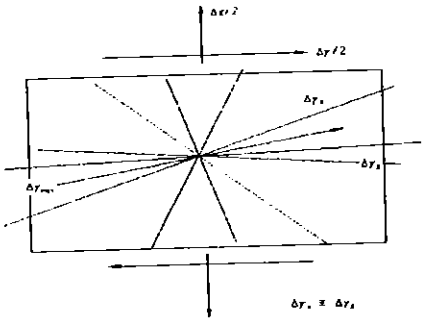

Fig.7B State of Shear strain at damageable plane under in-phase load(λ =1).

Fig.8A Slip lines under 90° out- of-phase load(λ =2).

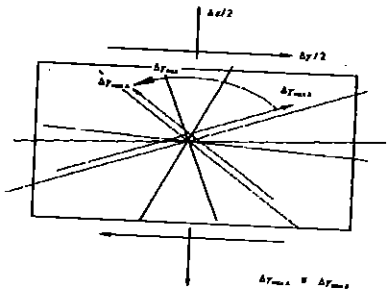

Fig.8B State of shear strain at damageable plane out-of- under 90° phase load(λ =2).

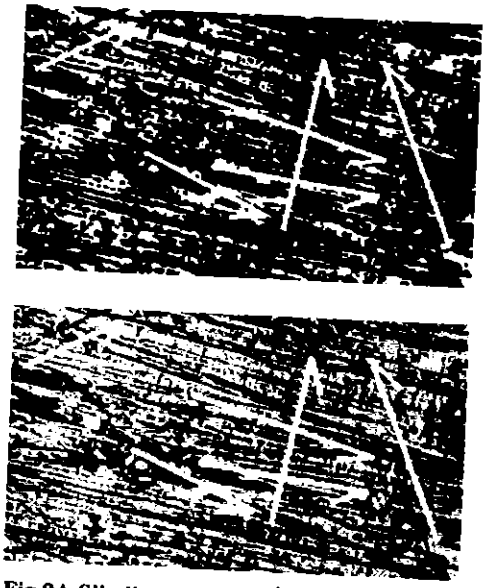

Fig.9A Slip lines under 90° out-of- phase load(λ =1).

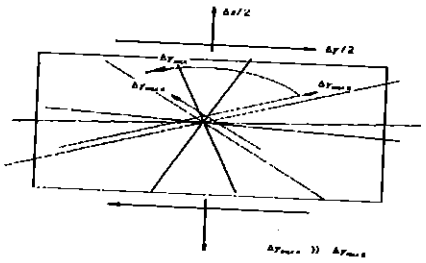

Fig.9B State of Shear strain at damageable plane under 90° out-of-phase load(λ =1).

(a) Torsion, $\Delta\gamma/2$=0.005, N_f=40,000 (b) In-phase, λ=1, $\Delta\varepsilon/2$=0.004, $\Delta\gamma/2$ =0.004, N_f=1443

Fig. 10 Slip lines under torsional & in-phase loaded specimen

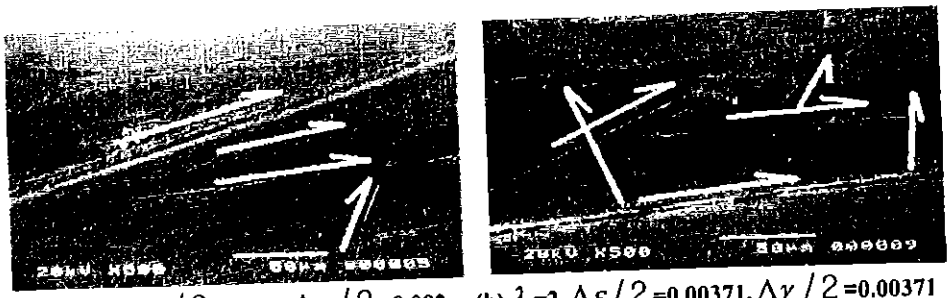

(a) λ=0.5, $\Delta\varepsilon/2$=0.004, $\Delta\gamma/2$=0.002 N_f=2790, (b) λ=2, $\Delta\varepsilon/2$=0.00371, $\Delta\gamma/2$=0.00371 N_f=1957

Fig. 11 Slip lines under 90o out-of-phase loaded specimen

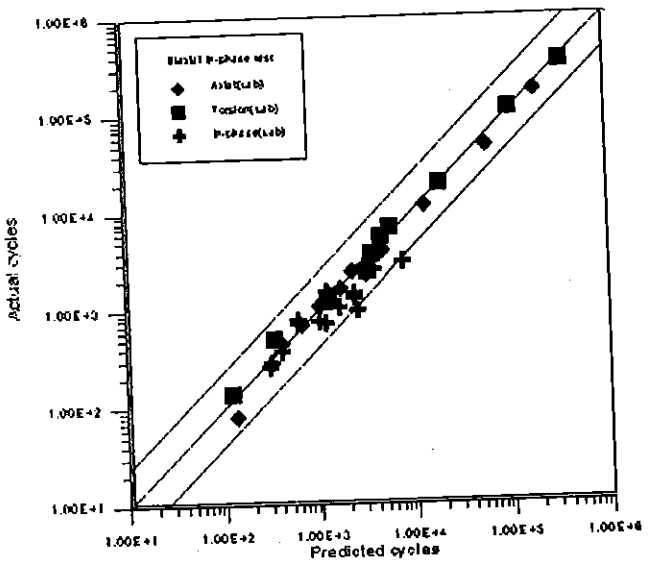

(a) Biaxial in-phase loading

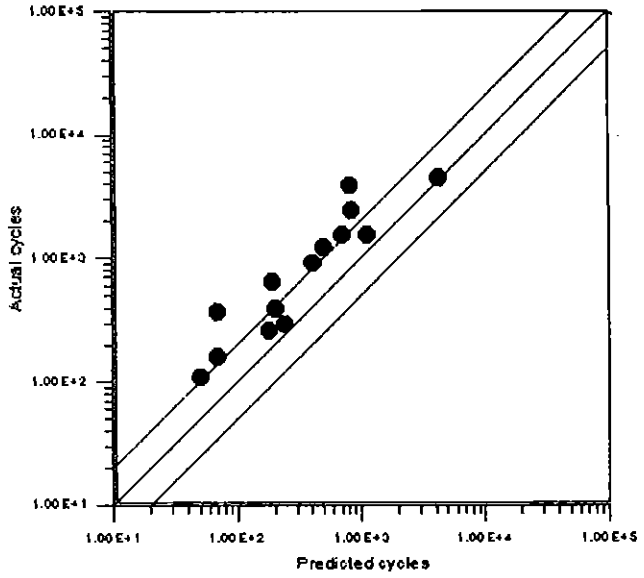

(b) Biaxial 90 deg. out-of-phase loading

Fig.12 Comparison of predicted lives by maximum shear strain and actual lives of Al7075-T651 under biaxial in-phase and 90 deg. out-of-phase loading

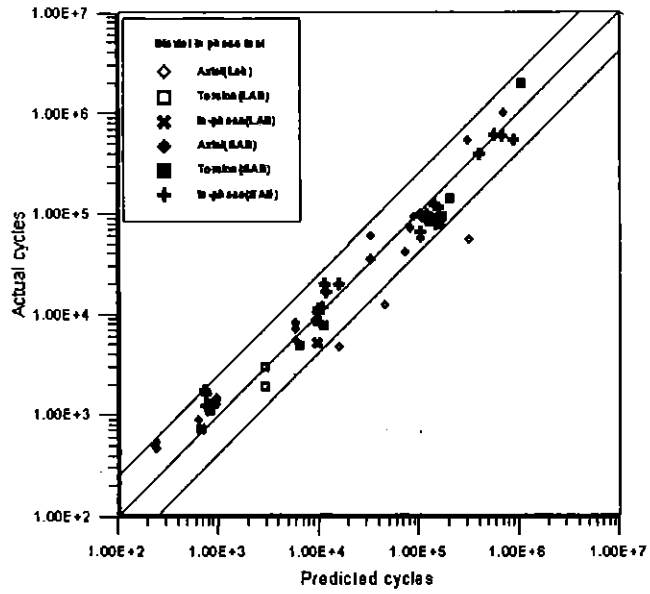

(a)Biaxial in-phase loading

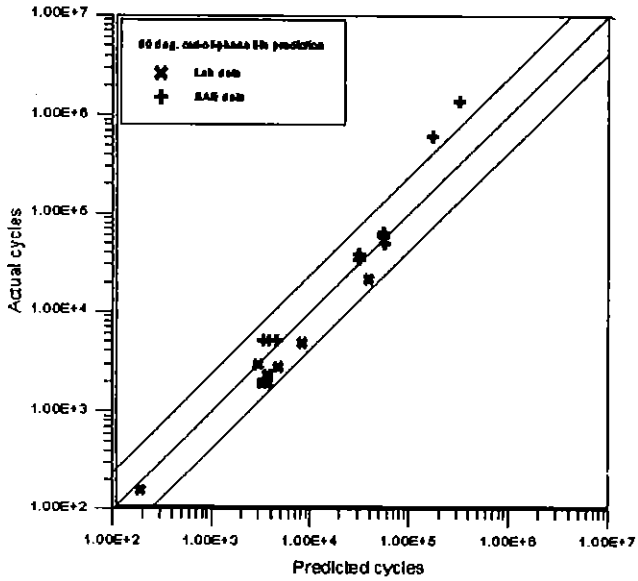

(b) Biaxial 90 deg. out-of-phase loading

Fig.13 Comparison of predicted lives by maximum shear strain and actual lives of 1045 steel under biaxial in-phase and 90 deg. out-of-phase loading

Life Prediction Of Biaxial In-phase & 90° Out-Of-Phase Loaded Specimen

The expected life based on proposed damage mechanism versus test results of Al7075-T651 is shown by Fig.12. The number of cycles at crack initiation predicted by the maximum shear strain theory was calculated as the function of N_f in Fig.12. The life of in-phase loading case was predicted with accuracy of 50-200%. But prediction life under 90 deg. out-of-phase loading was underestimated with accuracy of 100%-400%. The fatigue lives of 1045 steel were predicted by maximum shear strain[Fig.13]. The predicted fatigue lives are compared with actual lives of lab test data and SAE data. The prediction results in in-phase and 90° out-of-phase test show the accuracy of 2. The fatigue life range of 100,000-higher shows 3 times underestimated. This underestimation is from mechanism changing in fatigue damage. These results mean that the proposed damage mechanism is reasonable.

Equivalently Damaged Load Path Test of Al7075-T651

Two different kinds of load path were applied to the tubular specimen. In the case of circular path [Fig.14], damageable planes are chosen from the relative damage angle between main slip lines and the other slip lines. So, these four kinds of different load path

gives the same damage on each damageable plane. It was almost identical to the rectangular load path[Fig.15].The circular and rectangular load path was designed to give the same damage to the tubular specimen. The test results are given in Fig. 16. The test data show the same damage in the statistical point of view. It is concluded that the proposed damage mechanism is reasonable.

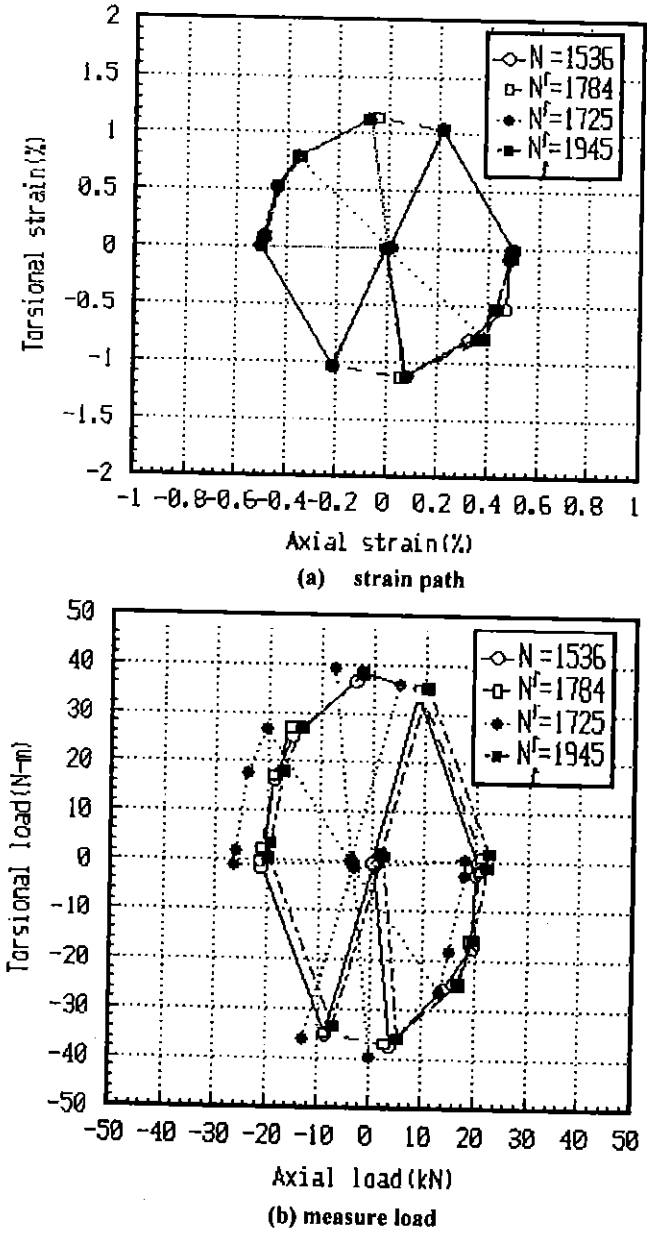

(a) strain path

(b) measure load

Fig.14 Equally damageable biaxial-circular load path

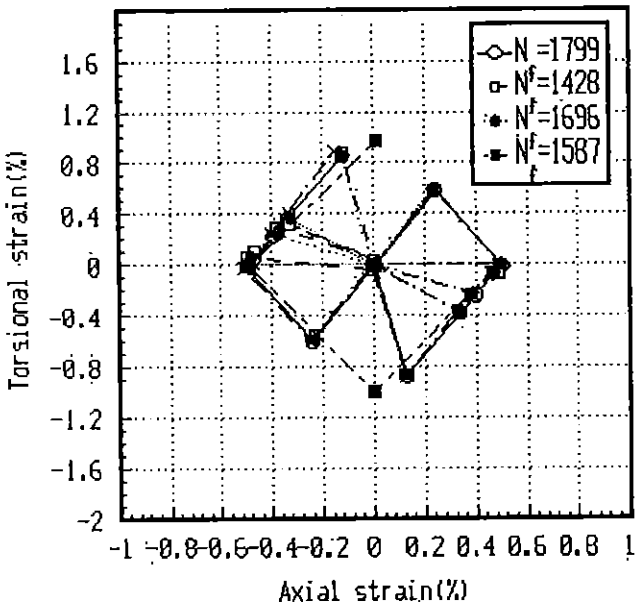

(a) strain path

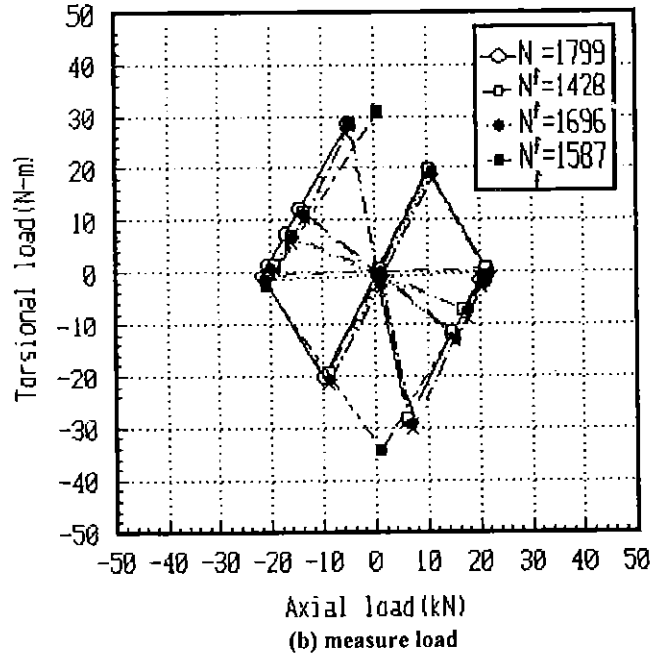

(b) measure load

Fig.15 Equally damageable biaxial-rectangular load path

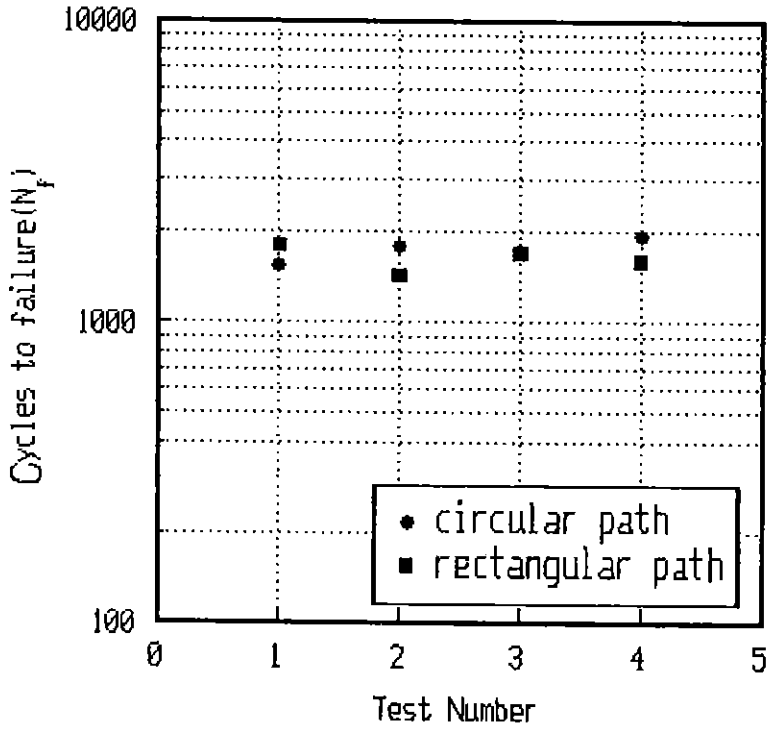

Fig.16 Comparison of tested lives by equally damageable load path

Biaxial Variable Sinusoidal & Random Load Test

Biaxial variable sinusoidal and random load paths were applied to the tubular specimen of 1045 steel. Biaxial variable sinusoidal load components variations and loading spectrum components are shown in Fig.17 and resultant plot of strain locus is shown in Fig.18. Biaxial variable random load components variations and loading spectrum's frequency scatters are shown in Fig.19 and resultant plot is shown in Fig.20. Fatigue lives prediction results are shown in Fig.21. In the case of variable sinusoidal load path, fatigue lives were predicted by maximum shear strain theory. The accuracy of fatigue life prediction results appeared to be conservative(predicted fatigue lives are 0.5-1 fold of experimental fatigue lives). In the case of variable random load paths, the accuracy of fatigue life prediction results appeared to be nearly 0.5 fold of experimental fatigue lives.

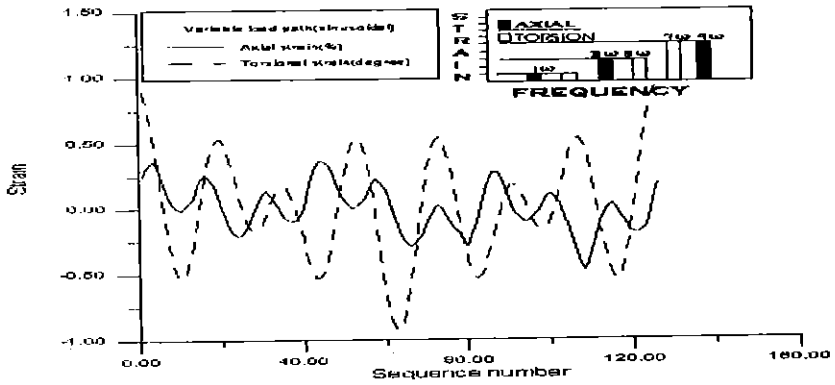

Fig.17 Axial and torsional strain variation under biaxial variable sinusoidal load path

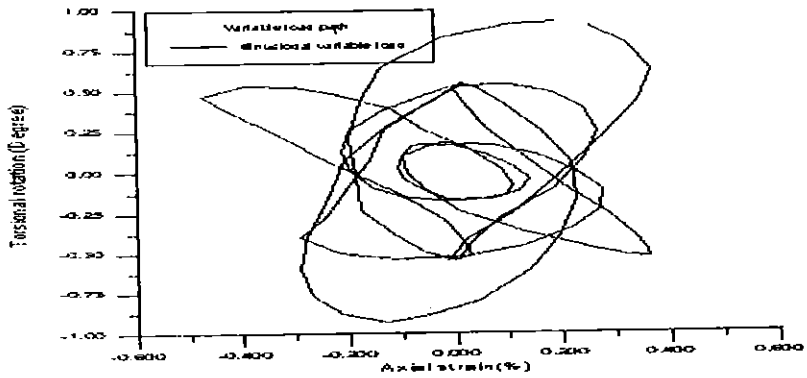

Fig.18 Plot of axial and torsional strain variation on xy-plane under biaxial variable random load path

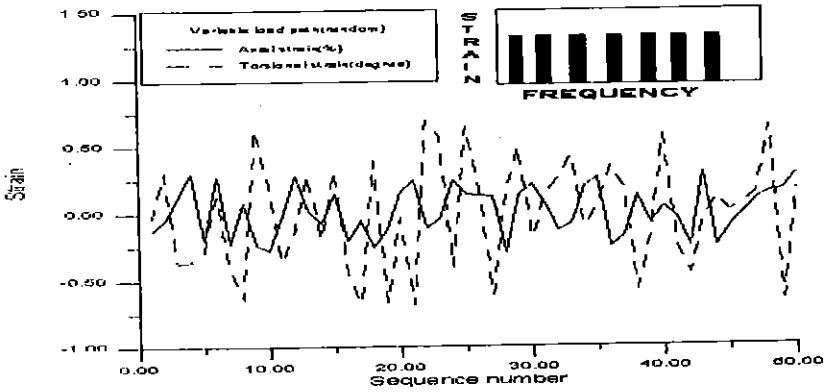

Fig.19 Axial and torsional strain variation under biaxial variable random load path

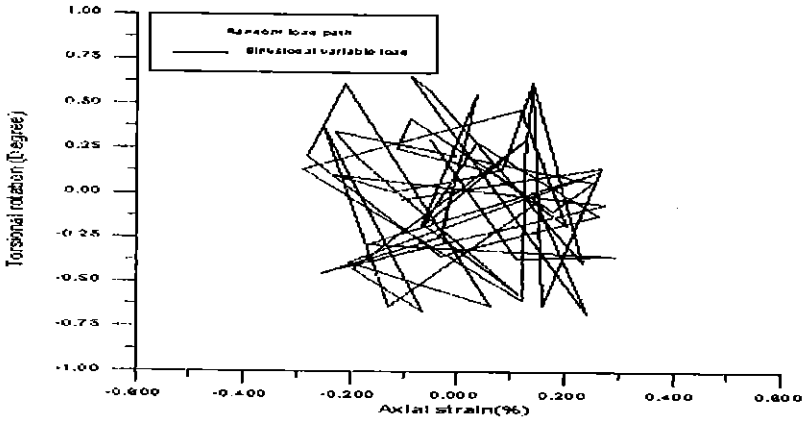

Fig.20 Plot of axial and torsional strain variation on xy-plane under biaxial variable random load path

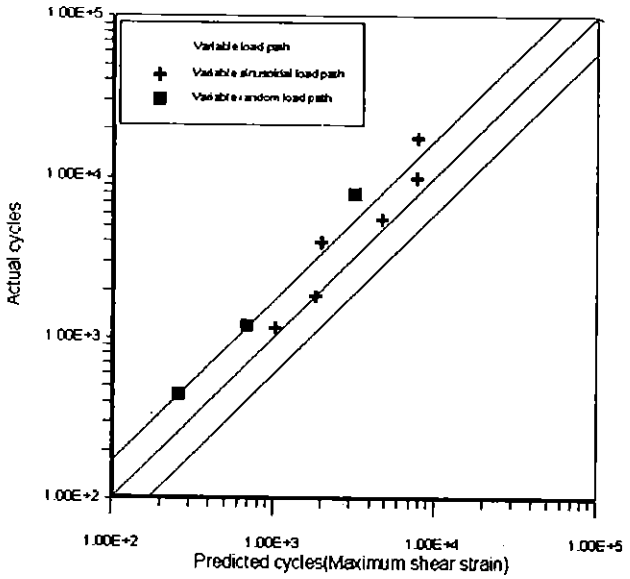

Fig.21 Fatigue life predictions under biaxial variable sinusoidal and random loads (based on maximum shear strain theory)

Conclusions

In this study, the following conclusions have been obtained.

1. Non-proportional load path effect of 90° out-of-phase loaded Al7075-T651 and 1045 steel materials depend on crystal structure.

2. The fatigue damage of multiaxially loaded materials with non zero plastic strain can be accounted by damageable plane assumption.

3. Biaxial low cycle random loading damage can be accounted by the proposed damage mechanism.

References

(1)Sakane M., Ohnami M., Swada M., 1987, Transaction of ASME, Journal of Engineering Materials and Technology, Vol.109, pp.236-243.
(2) Lhor R.D. and Ellison E.G., 1980, Fatigue Engng. Mater. Struct., Vol.3, No.1, pp1-pp17.(3) Socie D., 1987, Transaction of ASME, J. of Engng. Mater. and Technology, Vol.109, pp.293-298.
(4) Fatemi A. and Socie D.F., Fatigue Fracture Engng. Mater.,
(5)EllyinF. and Golos K., 1988, Transation of ASME, j.of Engng. Mater. and Technology, Vol.110, pp.63-68.
(6) Xia Z. and Ellyin F., 1991, J. of Applied Mechanics, Vol.58, pp.317-365.
(7)Doong S.H. and Socie D.F, 1991, Fatigue under Biaxial & Multiaxial loading, ESISO, Mechanical Engineering Publications, London, pp.305-320.
(8)Cailletaud G., Doquet V. and Pineau A., 1991, Fatigue under Biaxial & Multiaxial loading, ESISO, Mechanical Engineering Publications, London, pp.131-149.
(9) Dieter G.E., 1986, Mechanical Metallurgy, McGraw-Hill Inc., 3rd ed, pp.116.
(10)Oh S.J., Lee H.W., Jeon J.C., 1995, Transaction of the KSME, Vol.19, No.12, pp.3170-3176.
(11)Peter Kurath, 1989, Summary of Non-Hardened Notched Shaft Round Robin Program, Mutiaxial Fatigue, Analysis and Experiments, AE-14, SAE, pp.13-31